PCCP

Accepted Manuscript

ROYAL SOCIETY OF CHEMISTRY

www.rsc.org/pccp

Cite this: DOI: 10.1039/c0xx00000x

www.rsc.org/xxxxxx

ARTICLE TYPE

Influence of Counter-Anions During Electrochemical Deposition of ZnO on the Charge Transport Dynamics in Dye-Sensitized Solar Cells

Christoph Richter,[‡a] Max Beu[‡a] and Derck Schlettwein*[a]

Received (in XXX, XXX) Xth XXXXXXXXX 20XX, Accepted Xth XXXXXXXXX 20XX

DOI: 10.1039/b000000x

Porous ZnO/EosinY films have been electrochemically deposited by oxygen reduction in the presence of a zinc salt from EosinY-containing aqueous solutions, with either chloride or perchlorate as counter anion. EosinY was removed and the films were sensitised by D149. These electrodes were used for dye-sensitised solar cells (DSC) and charge transport in the porous network was studied by intensity modulated current/voltage spectroscopy (IMVS/IMPS) and electrochemical impedance spectroscopy (EIS) under illumination. Doping of ZnO during the electrodeposition could be proven by changes in the charge transport in ZnO and could be shown to occur when chloride was used as counter ion. By changing towards perchlorate as counter ion, on the other hand, a more reproducible occupation of trap levels was obtained at, however, slightly lower voltages in DSC whose origin is discussed in detail.

Introduction

ZnO-based dye-sensitized solar cells (DSC) have been discussed as an alternative to TiO_2-based DSC because of low-temperature-routes that are available to prepare crystalline ZnO thin films.[1,2] Different growth routes are known to influence the morphology of ZnO by adsorption of constituents to different ZnO surfaces[3] and we will show how also the recombination characteristics of ZnO-based DSC can be influenced by the growth route.

Electrodeposition of ZnO from an aqueous electrolyte containing Cl^- anions can be regarded an established way to prepare crystalline films at low temperature. In the presence of EosinY porous electrodes can be produced for ZnO-based DSCs.[4] With such state of the art electrodeposited ZnO sensitized by the indoline dye D149 efficiencies at 1 sun light intensity of up to 5.6 % were reported.[5] To reach such efficiency contact of the electrolyte with the back electrode needs to be suppressed by a compact blocking-layer which can also be prepared by electrodeposition.[6–8] The chosen growth route will also influence the quality of the blocking layer, but to our knowledge no detailed study of such blocking-layers exists. As an alternative, compact ZnO blocking-layers can also be achieved by other low temperature methods like sputtering[9,10] or chemical bath deposition.[11]

Charge transport in porous ZnO films has been studied by several authors in the past.[12–15] Mainly photocurrents induced by a laser flash were used to probe the distribution of defect states in ZnO and a large amount of defect states below the conduction band edge were detected. These defect states have a strong influence on the charge transport controlled by diffusion. A two-regime-model was developed which considers diffusion disturbed by trapping and by tunnelling between trap states which is widely accepted and used to describe electron transport in porous semiconductors.[16]

It was recently shown that details of the bath and conditions during electrodeposition of porous ZnO had a significant influence on the short circuit photocurrent density (J_{sc}), open circuit photo voltage (V_{oc}), fill factor (FF) and, consequently, on the conversion efficiency (η) in DSC, which was explained by differences in the concentration of surface defects.[17] Under typical deposition conditions doping interactions occur in a widely uncontrolled way. Albeit often leading to quite efficient cells, a low level of control can hamper technical applications. Cl is reported as an n-type dopant for compact electrodeposited ZnO, which leads to high free carrier concentrations.[18–23] An effective increase of the conduction band edge was observed, which was explained by a Burstein-Moss shift. The energetic distribution of the created defects was measured by comparing the intensity of the UV emission compared to the visible light emission. Deep defects created a strong emission in the visible part of the spectrum.[24] Doping reactions of oxide semiconductors by Cl are known also beyond the present case of ZnO for, e.g., SnO_2[25] and TiO_2,[26,27] where, however, Cl-doping led to narrowing of the band gap which was proposed to enhance the photocatalytic activity of TiO_2. By changing the counter anion from chloride to perchlorate during the electrodeposition of compact ZnO, Pauporté et al. observed a decrease of emission from deep defects and explained this by decreased doping of only 0.38 % Cl for samples deposited from a perchlorate-containing deposition bath compared to 3.3-4.0 % Cl for samples deposited from a chloride-containing deposition bath.[24] Hence, by simply changing the anion during electrodeposition of ZnO a decrease of defects can be achieved. The importance of a well-controlled growth was recently emphasized as an important criterion to

explain the fact that DSC based on ZnO lack behind the reported efficiencies for those based on TiO_2 despite comparable physical properties of the two semiconductors.[28,29]

In this work we transferred the above approach of using aqueous perchlorate-based solutions for the deposition of compact ZnO to the electrodeposition of porous ZnO applicable in DSC by use of the established structure-directing agent EosinY. We obtained electrodes with a well-defined density of states (DOS) and compare them to films from chloride-based solutions. A detailed study of the charge carrier recombination at the semiconductor/electrolyte interface was performed by intensity modulated voltage spectroscopy (IMVS)[30] and intensity modulated photocurrent spectroscopy (IMPS)[31] aside from classical current-voltage-analysis. Electron lifetimes and electron transit times were thereby obtained which were related to the charge recombination resistance (R_{rec}) and the chemical capacitance (C_μ) obtained by electrochemical impedance spectroscopy (EIS).[32] Insight into the distribution of the DOS provides a valuable basis to understand the differences in charge transport and recombination characteristics, a fundamental prerequisite for further improvement of the efficiency in DSC based on ZnO.

Experimental

Electrodeposition of porous ZnO electrodes

Glass slides with F-doped tin oxide (FTO, 7Ω/sq, Sigma-Aldrich) were subsequently cleaned in aqueous detergent solution, acetone and isopropanol (Roth) in an ultrasonic bath for 15 min each. The FTO-sample was mounted on a rotating disc electrode (RDE) rotating at 500 rpm. Electrodeposition of ZnO was realised by a three-electrode setup in a glass vessel at 70 °C. The electrolyte consisted of an aqueous solution of 0.1 M KCl or 0.1 M $LiClO_4$ (Sigma-Aldrich) which was saturated with oxygen by intense purging for at least 15 min before each deposition. Independence of the reactions from the cation was proven by control experiments with LiCl for which films did not reveal any difference to those prepared with KCl. The counter electrode consisted of a platinum wire. A RedRod Ag/AgCl (Radiometer analytical) was used as reference electrode. Prior to electrodeposition of ZnO the FTO-substrate was pre-electrolyzed for 30 min at a potential of -1060 mV. Then $ZnCl_2$ (Merck) or $ZnClO_4$ (Sigma-Aldrich) was injected from a stock solution to achieve a concentration of 5 mM $ZnCl_2$ or 5 mM $ZnClO_4$ in the deposition bath. A compact ZnO blocking layer of about 800 nm was deposited for 10 min. Subsequently the platinum counter electrode was replaced by a zinc wire (99.9 %, GoodFellow) and EosinY (Sigma-Aldrich) was added to achieve a concentration of 75 µM EosinY. The deposition was continued at a potential of -960 mV for 20 min. Afterwards, the EosinY was desorbed in an aqueous solution of 10.5 pH KOH for 12 h. Alternatively, a compact ZnO layer was sputter-deposited (Leybold-Heraus Z400) on the substrate instead of electrodepositing ZnO. Recipient pressure of Argon (Air Liquide, 5.0) was lower than 10^{-4} mbar. Films were prepared at a sputter rate of 12 nm/min. The resulting blocking layer thickness was about 180 nm.

Characterisation of ZnO

The morphology was analyzed by Scanning-Electron Microscopy (SEM) in a Zeiss Merlin instrument at 5 kV acceleration voltage, 120 pA emission current and 2-3 mm working distance with an in-lens detector. An EDX detector (Oxford Instruments) was used to analyse the elemental composition of films.

X-Ray Diffraction (XRD) measurements were carried out with a PANalytical X'Pert Pro setup equipped with a Cu Kα X-ray tube in Bragg-Brentano geometry. Samples were mounted on a sample holder and rotated during measurements.

To determine the inner surface area, the sensitizer D149 was desorbed from electrodes in a DMF solution overnight. The electrodes were then rinsed with ethanol and water and dried in a nitrogen stream. EosinY was then adsorbed to the electrodes as a probe molecule by refluxing the films for 30 min in a 1 mM ethanolic solution of EosinY. It was then desorbed again from the films into an aqueous KOH solution of pH 10.5 for 12 h. The amount of EosinY molecules was calculated from the optical absorbance of this solution at 512 nm. The molar extinction coefficient at 512 nm is 91.600 M^{-1} cm^{-1}. Assuming an occupied area of 3.32 nm^2 for one molecule of EosinY and a porosity of 60 %[33,34] of the films the inner surface area was calculated from the average film thickness determined by an Alpha step 100 (KLA Tencor) and referred to the mass of the films based on the known density ρ_{ZnO}= 5.61 gcm^{-3}.[35]

Preparation of DSC

ZnO films were dried at 150 °C for 30 min and illuminated by UV-light for 30 min to hydroxylate the surface.[36] The samples were immersed in a solution of 0.5 mM D149 and 1 mM lithocholic acid in a 1:1 vol% mixture of acetonitrile / tert-butanol for 15 min and rinsed with ethanol to remove any excess dye. The films were dried in a nitrogen stream. The counter electrode was prepared by spreading 20 µL of 5 mM H_2PtCl_6 (Sigma-Aldrich) dissolved in ethanol on a FTO-substrate and subsequent annealing at 400 °C for 30 min. Both electrodes were sealed together with a Surlyn foil (jurasol b, jura-plast GmbH). The electrolyte consisting of 0.5 M 1-methyl-3-propylimidazolium iodide (Sigma-Aldrich) and 0.05 M iodine (Scharlau) dissolved in acetonitrile was injected into the cell through two predrilled holes. The holes were then sealed with a piece of Surlyn foil and a cover slip. At least two specimen were prepared for each type of cell.

Photoelectrochemical characterisation

Photoelectrochemical measurements were carried out under illumination by an Oriel 150 W Xenon arc lamp equipped with an AM 1.5 solar filter. The light intensity was calibrated with a pyranometer (EKO Instruments) to 100 mW/cm^2. The impedance under 1 sun illumination was measured with a Zahner IM6 (Zahner Elektrik GmbH) potentiostat with an amplitude of 10 mV and a step width of 20 mV from V_{OC} until -0.3 V and with an amplitude of 20 mV and a step width of 50 mV further to 0 V. For the interpretation and fitting of the data derived from impedance spectroscopy under one sun the well-established equivalent circuit diagram for DSCs, presented in figure (ESI Fig. 1), was used.[32] IMVS and IMPS measurements were carried out with a Zahner CIMPS system (Zahner Elektrik GmbH) using

a red light emitting diode (627 nm) that served as the background light intensity onto which a small sinusoidal amplitude was superimposed with less than 10 % of the background intensity. A red light emitting diode was chosen to assure uniform excitation throughout the sample by weak absorption.

Results and Discussion

Morphological properties and crystallinity

In Fig. 1 (left) a scanning-electron microscopy (SEM) image of a ZnO sample deposited from a chloride-containing deposition bath ($ZnO(Cl^-)$) right after desorption of EosinY is depicted. Fig. 1 (right) shows an image of an analogously treated ZnO sample prepared from a perchlorate-containing deposition bath ($ZnO(ClO_4^-)$). Both samples have an open porous structure with pores of around 10 nm diameter. A detailed observation at higher magnification also showed no significant difference between both preparation methods. The inner surface is accessible for an electrolyte and in former studies the cauliflower-like porosity has been described in detail for ($ZnO(Cl^-)$) which has proven to be a promising electrode for DSCs.[37] The thickness of ZnO in our experiments was roughly 4.5 µm for both preparation methods. To determine the inner surface of the porous ZnO films we conducted EosinY adsorption/desorption measurements and obtained almost identical values for the inner surface of 180.3 ± 1.2 m^2/g for $ZnO(Cl^-)$ and 180.8 ± 1.3 m^2/g for $ZnO(ClO_4^-)$. Differences in charge carrier recombination characteristics as discussed below therefore should not be influenced by variations in surface area.

Since the crystalline orientation of ZnO may play an important role for the device parameters,[38,39] we conducted x-ray diffraction measurements (XRD) to study the film texture by the relative intensity of signals (Fig. 2). ZnO from both deposition baths showed a clear c-axis orientation normal to the substrate plane prominent in the (002) reflex (Fig. 2) which is typical for porous ZnO films electrodeposited in the presence of EosinY.[40] The higher intensity relative to the other diffraction reflexes for $ZnO(ClO_4^-)$ shows more pronounced crystalline orientation along the (002) lattice plane compared to $ZnO(Cl^-)$. Further, $ZnO(ClO_4^-)$ samples showed a slightly higher crystallinity compared to the $ZnO(Cl^-)$ samples evidenced by a decreased full width at half maximum of the (002) diffraction reflex for $ZnO(ClO_4^-)$.

Photovoltaic characteristics

The established method to prepare high efficiency ZnO-based DSCs by electrodeposition from a chloride-containing bath was varied to detect critical parameters of preparation and to thereby provide parameters for further optimization. We prepared ZnO-DSCs: (1) a blocking- and a porous layer electrodeposited from a perchlorate-containing bath ($EC/ZnO(ClO_4^-)$), (2) a sputtered blocking-layer and a porous layer electrodeposited from a perchlorate-containing bath ($SP/ZnO(ClO_4^-)$), (3) a sputtered blocking-layer and a porous layer electrodeposited from a chloride-containing bath ($SP/ZnO(Cl^-)$) to compare with (4) the established DSCs consisting of a blocking- and a porous layer electrodeposited from a chloride-containing bath ($EC/ZnO(Cl^-)$). For the direct comparison of the sensitized porous layers we have

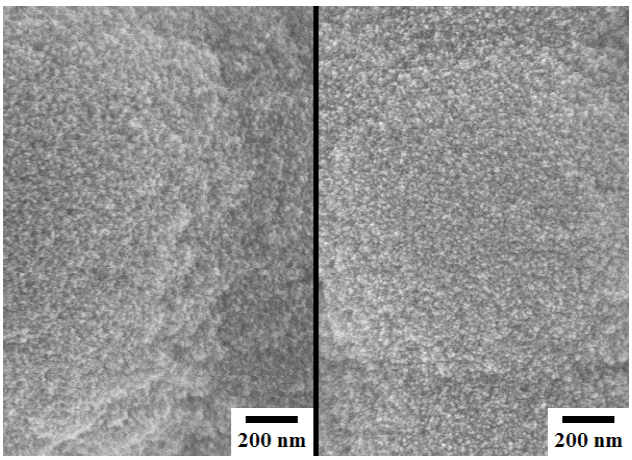

Fig. 1 Scanning electron microscopy of porous ZnO deposited from a chloride-containing (left) or perchlorate-containing electrolyte (right).

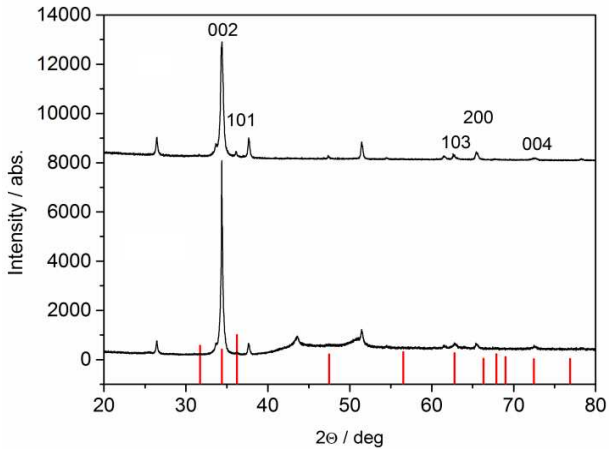

Fig. 2 X-ray diffractograms for porous ZnO deposited from a chloride-containing (bottom) or perchlorate-containing electrolyte (top). Red lines mark reflection peaks of crystalline ZnO.[41]

chosen samples with identical sputter deposited blocking-layers (type 2, $SP/ZnO(ClO_4^-)$) and (type 3, $SP/ZnO(Cl^-)$) to exclude the influence of the different ions in the electrodeposited blocking-layers. The sputtered compact ZnO is at least equally suited as electrodeposited compact ZnO to work as a blocking layer to suppress recombination at the transparent conductive oxide/electrolyte interface (Table 1 and ESI Fig. 2). Cells based on the sputtered compact ZnO therefore led to similar or better performance than those using electrodeposited blocking layers (Table 1). For improved clarity in the presentation we have chosen one representative $SP/ZnO(Cl^-)$ and one representative $SP/ZnO(ClO_4^-)$ sample for the discussion of detailed device parameters. The IV-curves of the two samples measured under one sun are presented in Fig. 3 showing almost ideal DSC characteristics. The corresponding performance parameters of these (in boldface) and the other cells prepared are listed in Table 1. All samples were treated identically to exclude any other effects aside from the different deposition baths. The differences in the short circuit current density (J_{sc}) are within the typical range mainly caused by variations in the amount of adsorbed dye. All samples showed high fill factors of over 70 % typical for highly efficient DSCs as also reported in the literature.[42] $ZnO(Cl^-)$ samples showed a V_{oc} increased by around 30-40 mV

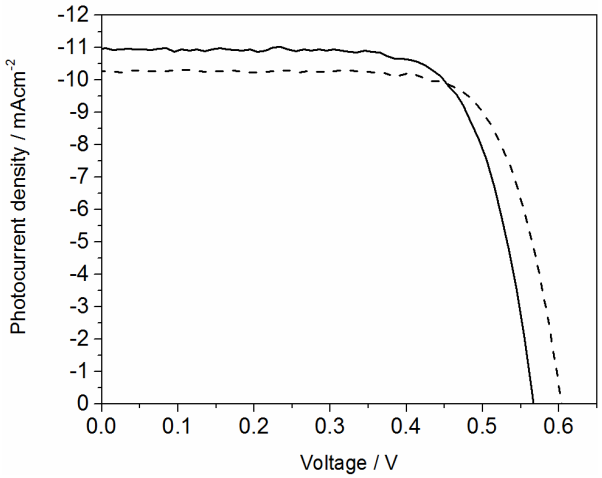

Fig. 3 IV-curves under AM 1.5 conditions of DSCs made of porous ZnO deposited from Cl^--containing (– – –) or ClO_4^--containing electrolyte (——) onto sputter-deposited blocking-layers.

compared to the $ZnO(ClO_4^-)$ samples. This observation can be explained by doping reactions, leading to an increased occupation of either defect states in the band gap or of states in the conduction band (Burstein-Moss shift). In both cases the Fermi level of the semiconductor would be shifted to higher energies resulting in an increased V_{oc} and a shift in the chemical capacitance. We conducted EDX measurements to check for differences in chemical doping. For both kinds of samples a Cl-content around 0.16 at. % was found. A detailed comparison for all atomic percentages is listed in ESI Tab. 1. Only in the case of the films from the chloride-containing bath, however, Cl led to the observed changes in the electronic system of the electrodes as seen in the changes of V_{oc} and explicitly detected by a significantly wider band gap (Burstein-Moss shift) directly measured by optical absorbance of the films (ESI fig. 4). From the Tauc-Plot optical band gaps of 3.51 eV and 3.39 eV were measured for $ZnO(Cl^-)$ and $ZnO(ClO_4^-)$, respectively. Non-targeted doping of ZnO therefore led to a significant variation in V_{oc} for the $ZnO(Cl^-)$ samples of this series (ESI fig. 2) and an increased occupation of states in the CB of ZnO was confirmed by a Burstein-Moss-shift which was not observed for $ZnO(ClO_4^-)$. V_{oc} appeared to be more constant for $ZnO(ClO_4^-)$ within our series. Since EDX analysis did not reveal a significantly higher Cl-content in $ZnO(Cl^-)$ compared to $ZnO(ClO_4^-)$ no proof can be given for Cl-doping in $ZnO(Cl^-)$ which would provide the most straightforward explanation. The observed changes in the photodynamics could also be a consequence of increased doping by native defects established during the electrodeposition in the presence of Cl^-.

Recombination

The chemical capacitance C_μ was determined from EIS measurements at the cells. The applied forward bias voltage was corrected for the series resistance of the cells to obtain V_f. The semilogarithmic plot of C_μ vs. V_f in Fig. 4 allows to analyse the trap distribution in the electrodes. In the section where C_μ is exponentially dependant on V_f a linear fit of the semi logarithmic plot according to equation 1

$$C_\mu = C_{o,\mu} \exp\left(\frac{\alpha e V_f}{k_B T}\right) \quad (1)$$

allowed to determine the parameter α characteristic for the width of the trap distribution below the conduction band edge for the $ZnO(ClO_4^-)$ and the $ZnO(Cl^-)$ samples. The similarity in α (see Table 2) implies a similar width of the distribution of defect

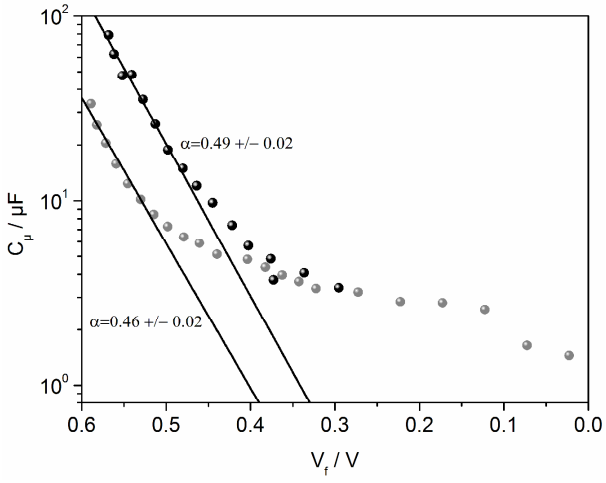

Fig. 4 Chemical capacitance calculated by fitting EIS data (AM 1.5) to the equivalent circuit (EIS Fig. 3) for cells constructed from porous ZnO (Fig. 3) either deposited from Cl^--containing (●) or ClO_4^--containing electrolyte (●). The lines represent exponential fits according to eq. (1) to the capacitance at higher voltages providing the corresponding values of α indicated in the plot..

states for both preparation methods, therefore allowing a correction for the conduction band offset. The voltage difference of both lines is characteristic for a conduction band edge shift of 70 mV. A shift caused by excessive doping (Burstein-Moss-shift) was already discussed above as a possible origin for the higher V_{oc} for $ZnO(Cl^-)$. Since V_{oc}, however, could also be altered by a decreased recombination rate the latter has to be considered for a conclusive discussion.

Table 1 Average values of the photovoltaic characteristics with standard deviation under AM 1.5 conditions of DSC of porous ZnO electrodeposited from a perchlorate containing electrolyte ($ZnO(ClO_4^-)$) or from a chloride-containing electrolyte ($ZnO(Cl^-)$) on either a sputter-deposited blocking-layer (SP) or an electrodeposited blocking layer (EC). Samples chosen for discussion and illustrations below in bold.

Sample	η / %	J_{sc} / mA cm^{-2}	V_{oc} / V	FF / %
EC/$ZnO(ClO_4^-)$	4.05±0.35	10.01±0.98	0.580±0.01	71±1
SP/$ZnO(ClO_4^-)$	**4.36**±0.21	**10.54**±0.63	**0.568**±0.001	**73**±1
EC/$ZnO(Cl^-)$	4.83±0.31	11.19±0.95	0.613±0.004	71±2
SP/$ZnO(Cl^-)$	**4.60**±0.04	**10.55**±0.40	**0.600**±0.01	**75**±3

An important tool to correctly evaluate the recombination rate is to plot the recombination resistances of different devices at the same voltage relative to the conduction band edge. Fig. 5 shows a semi-logarithmic plot of the resistance for charge recombination R_{rec} plotted against the voltage corrected for different conduction band positions (V_{CB}) determined in (Fig. 4).[32,43] R_{rec} was directly obtained from fits to the Nyquist-plots of the spectra by the width of the second arc. For all samples the transport resistance R_{tr}

which describes the conductivity of the semiconductor was negligible. The R_{rec} values for ZnO(ClO_4^-) are larger than the values for ZnO(Cl^-). This is indicating that less surface defects are present in the ZnO(ClO_4^-) sample since R_{rec} is very sensitive to surface defects which promote recombination.[44]

Therefore the observed change in V_{oc} of about 30-40 mV among ZnO(ClO_4^-) and ZnO(Cl^-) (Table 1) is found smaller than the shift of the conduction band edge of about 70 mV. The observed difference in V_{oc} is therefore caused by a shift of the conduction band edge by the Burstein-Moss-effect as already discussed above superimposed to a change in the recombination rate[32] since a smaller R_{rec} was found for ZnO(Cl^-) (Fig. 5).

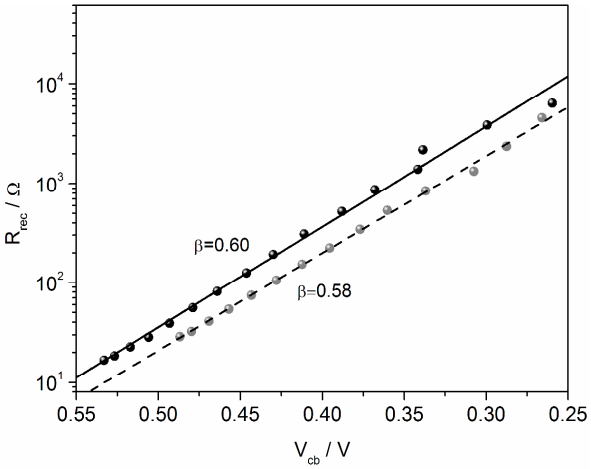

Fig. 5 Recombination resistance calculated by fitting EIS data (AM 1.5 conditions) to the equivalent circuit (EIS Fig. 3) for cells constructed from porous ZnO (Fig. 3) either deposited from Cl^--containing (●) or ClO_4^--containing electrolyte (●). The lines represent exponential fits according to eq. (2) providing the corresponding β-values.

Table 2 α- and β- values determined from EIS measurements for cells constructed from porous ZnO (see Fig. 3) either deposited from Cl^--containing or ClO_4^--containing electrolytes.

Sample	α	β
SP/ZnO(Cl^-)	0.46 +/- 0.02	0.58
SP/ZnO(ClO_4^-)	0.49 +/- 0.02	0.60

From the slope of the semi logarithmic plot one can obtain the β-parameter by a linear fit according to equation 2.

$$R_{rec} = R_{0,rec} \exp\left(-\frac{\beta e V}{k_B T}\right) \qquad (2)$$

e describes the elementary charge, V the inner voltage of the cell, k_B the Boltzmann constant, T the temperature and β stands for the non-linearity of the reaction order of the recombination reaction at the semiconductor/electrolyte interface.[32] Almost constant β-values of 0.60 for ZnO(ClO_4^-) and 0.58 for ZnO(Cl^-) were obtained confirming the similarity of the materials aside from different extent of doping.

Electron lifetimes and transit times

IMVS and IMPS measurements were conducted to study the influence of the different growth conditions on the transport properties in the porous sensitized ZnO films. The electron lifetimes τ_n and transit times τ_D were obtained by fitting of the imaginary part of the response spectra as described in detail elsewhere.[30,31] In Fig. 6 τ_n is plotted against the incident light intensity. The sample deposited from a perchlorate-containing deposition bath showed an enhanced τ_n over the whole measurement range in comparison to the sample deposited from a chloride-containing deposition bath. This finding can be explained by the trapping –detrapping model in which it is assumed that under open circuit conditions trapping and detrapping of electrons is fast compared to recombination reactions with the electrolyte or electron transport along theporous network. Recombination reactions mediated trough trap states are neglected in this model.[44] τ_n is then given by

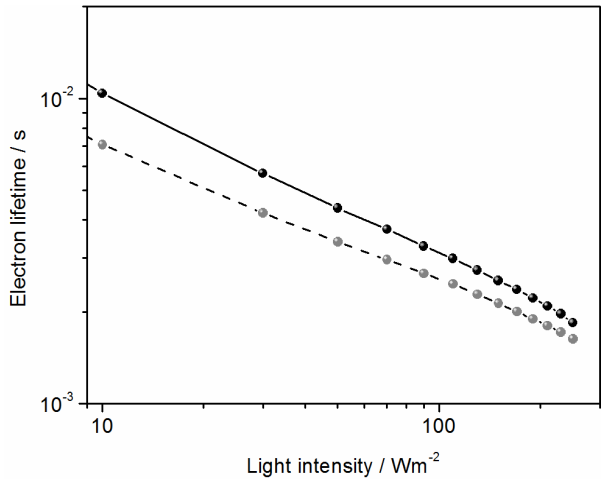

Fig. 6 Electron lifetime τ_n measured with IMVS depending on backlight intensity for cells constructed from porous ZnO (Fig. 3) either deposited from Cl^--containing(- ● -) or ClO_4^--containing electrolyte (- ● -).

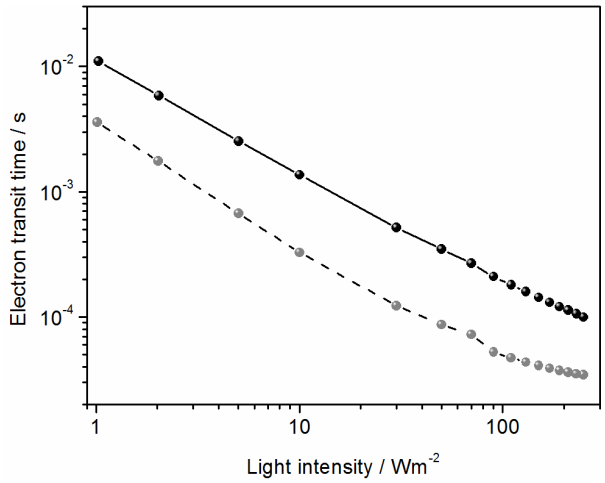

Fig. 7 Electron transit times measured with IMPS depending on backlight intensity for cells constructed from porous ZnO (Fig. 3) either deposited from Cl^--containing (- ● -) or ClO_4^--containing electrolyte (- ● -).

$$\tau_n = \left(1 + \frac{C_{\mu,traps}}{C_{\mu,CB}}\right)\tau_f \qquad (3)$$

with τ_f corresponding to the free electron lifetime in the

conduction band, $C_{\mu,traps}$ to the chemical capacitance of unfilled trap states and $C_{\mu,CB}$ to accessible conduction band states in the semiconductor. For a given mobility of electrons in the conduction band the ratio between the two chemical capacities determines the observed τ_n. Doping of ZnO decreases $C_{\mu,traps}$ more than $C_{\mu,CB}$ by increasing the electron density in the semiconductor and, hence, predominantly increasing the occupation of traps below the conduction band. This leads to a strongly decreased $C_{\mu,traps}$ (Fig. 4) at only slightly decreased $C_{\mu,CB}$ and to a thereby decreased τ_n since the trapping probability for

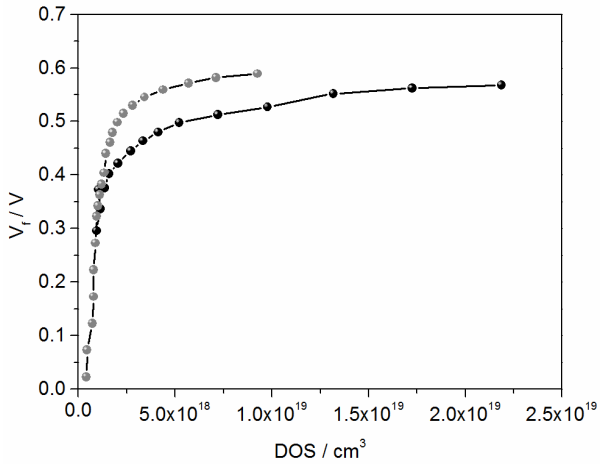

Fig. 8 Internal voltage plotted against the density of states for cells constructed from porous ZnO (Fig. 3) deposited from Cl^- containing electrolyte (- ● -) or from a ClO_4^- containing electrolyte (- ◕ -)

additional light-induced charge carriers is decreased. In the case of films deposited from a perchlorate bath considerably less doping leads to a larger $C_{\mu,traps}/C_{\mu,CB}$ which results in a higher τ_n (Fig. 6).

The electron transit times τ_D determined under short-circuit of the cells are shown in Fig. 7, also dependent on the incident light intensity. It can be assumed that at short circuit trapping and detrapping of electrons is no longer fast compared to their transport along the porous network and, hence, the resulting τ_D is decreased by a decreased probability of trapping events. Since the trapping probability is mainly determined by the concentration of unoccupied trap states, a discussion of the observed density of localized (trap) states (DOS) in the samples is needed.

Distribution of states determining recombination and electron transport

Since $C_{\mu,traps} >> C_{\mu,CB}$ it is possible to calculate the DOS from C_μ by the formula

$$DOS = \frac{C_\mu}{eAd(1-p)} \quad (4)$$

where A is the geometric area of the active layer of the DSC, d the thickness of the active layer and p the porosity of the porous ZnO layer. p is assumed to be 0.6[33,34] as typical for electrodeposited porous ZnO in the presence of EosinY which is consistent with the SEM of Fig. 1.[17,45,34],

In Fig. 8 the DOS thus calculated from the experimental values of C_μ are presented. The samples deposited from a chloride-containing deposition bath show a lower DOS at a given V_f. Since a constant distribution (β) of DOS (V_{CB}) has been found (Fig. 5) this means that ZnO (Cl^-) offers less unoccupied trap states at a given V_f consistent with the shorter τ_n and decreased τ_D for these samples. In the case of ZnO(Cl^-) the trap states are filled to higher occupancy at a given corrected voltage V_f (Fig. 8). This means that less traps are unoccupied in ZnO(Cl^-) leading to fewer trapping events. Therefore τ_n is decreased (Fig. 6, eq. 3) and charge carriers can move faster resulting in a shorter transit time τ_D (Fig. 7).

In ZnO(Cl^-) the occupation of trap states in the gap and of states in the CB is increased by Cl-doping or native defects. Thus the DOS is shifted to lower values at a given inner cell voltage V_f explaining the lower τ_n and the decreased τ_D. The non-targeted and poorly controlled extent of such doping leads to a higher variation in the occupation of trap levels in ZnO(Cl^-) compared to ZnO(ClO_4^-). The latter show widely constant DOS for preparation either on sputter-deposited or electrochemically deposited blocking layers (ESI Fig. 3).

Conclusions

As an alternative to the established deposition from a chloride-containing deposition bath, nanoporous ZnO films can also successfully be electrodeposited from a perchlorate-based deposition solution. The morphology of the obtained ZnO is determined by EosinY present in both solutions and therefore does not differ significantly. Good crystallinity and preferred c-axis orientation is observed in both cases. Thorough investigation of DSCs prepared from these films by IV measurements, impedance spectroscopy and IMVS/IMPS, however, revealed significant differences. The density of occupied trap states is strongly influenced by the chosen growth route for ZnO affecting the charge transport dynamics in the porous semiconductor network. By choice of the deposition bath one can directly influence the electron lifetime τ_n and the electron transit time τ_D. Doping of ZnO occurs during electrodeposition from chloride-containing solutions but a similar reaction was not observed when a perchlorate-based solution was used despite the detection of Cl on both kinds of films. Such doping in ZnO(Cl^-) leads to a decreased τ_D at, however, also decreased τ_n. Thus special attention should be paid to doping during the electrodeposition of ZnO. Electrodeposited porous ZnO from perchlorate-containing baths is characterized by a more reproducible trap occupation. For further studies these findings open the possibility to control and deliberately vary the doping of ZnO opening an interesting way to further improve ZnO-based dye-sensitised solar cells and mesostructured solar cells in general.

Acknowledgments

Financial support by the German Federal Ministry of Education and Research (BMBF) within the project KorTeSo (16SV4042) and support within the LOEWE program of excellence of the Federal State of Hessen (project initiative STORE-E) are gratefully acknowledged. The authors are grateful to H. Miura (Chemicrea Co., Japan) for providing the sensitizer D149.

Notes and references

[a] *Institute of Applied Physics, Justus-Liebig-University, Heinrich-Buff-Ring 16, 35392 Gießen, Germany. Fax: +49 641 99 33409; Tel:+49 641 99 33401; E-mail: schlettwein@uni-giessen.de*

† Electronic Supplementary Information (ESI) available: [Includes supplementary IV-curves, comparison of DOS and equivalent circuit for EIS, EDX analysis of films as well as optical analysis of the apparent band gap]. See DOI: 10.1039/b000000x/

‡ CR and MB performed all experiments and data analysis of this work at equal share.

* DS supervised the work and coordinated the discussion leading to this article, author to whom correspondence should be addressed.

1. S. Peulon and D. Lincot, *Adv. Mater.*, 1996, **8**, 166–170.
2. M. Izaki and T. Omi, *Appl. Phys. Lett.*, 1996, **68**, 2439.
3. D. Lincot, *MRS Bull.*, 2011, **35**, 778–789.
4. T. Yoshida, K. Terada, D. Schlettwein, T. Oekermann, T. Sugiura, and H. Minoura, *Adv. Mater.*, 2000, **12**, 1214–1217.
5. T. Yoshida, J. Zhang, D. Komatsu, S. Sawatani, H. Minoura, T. Pauporté, D. Lincot, T. Oekermann, D. Schlettwein, H. Tada, D. Wöhrle, K. Funabiki, M. Matsui, H. Miura, and H. Yanagi, *Adv. Funct. Mater.*, 2009, **19**, 17–43.
6. Y. Sakuragi, X.-F. Wang, H. Miura, M. Matsui, and T. Yoshida, *J. Photochem. Photobiol. A Chem.*, 2010, **216**, 1–7.
7. K. Ichinose, T. Inomata, H. Masuda, and T. Yoshida, *J. Photochem. Photobiol. A Chem.*, 2012, **242**, 67–71.
8. C. Magne, M. Urien, and T. Pauporté, *RSC Adv.*, 2013, **3**, 6315.
9. E. M. C. Fortunato, P. M. C. Barquinha, A. C. M. B. G. Pimentel, A. M. F. Gonçalves, A. J. S. Marques, L. M. N. Pereira, and R. F. P. Martins, *Adv. Mater.*, 2005, **17**, 590–594.
10. P. F. Carcia, R. S. McLean, M. H. Reilly, and J. Nunes G., *Appl. Phys. Lett.*, 2003, **82**, 1117–1119.
11. X. D. Gao, X. M. Li, and W. D. Yu, *J. Solid State Chem.*, 2004, **177**, 3830–3834.
12. S. Hotchandani and P. V Kamat, *J. Electrochem. Soc.* , 1992, **139** , 1630–1634.
13. P. Hoyer and H. Weller, *J. Phys. Chem.*, 1995, **99**, 14096–14100.
14. A. Solbrand, K. Keis, S. Södergren, H. Lindström, S.-E. Lindquist, and A. Hagfeldt, *Sol. Energy Mater. Sol. Cells*, 2000, **60**, 181–193.
15. A. Solbrand, A. Henningsson, S. Södergren, H. Lindström, A. Hagfeldt, and S.-E. Lindquist, *J. Phys. Chem. B*, 1999, **103**, 1078–1083.
16. J. Nelson, S. A. Haque, D. R. Klug, and J. R. Durrant, *Phys. Rev. B*, 2001, **63**, 205321.
17. C. Magne, T. Moehl, M. Urien, M. Grätzel, and T. Pauporté, *J. Mater. Chem. A*, 2013, **1**, 2079.
18. R. Salazar, C. Lévy-Clément, and V. Ivanova, *Electrochim. Acta*, 2012, **78**, 547–556.
19. O. Lupan, T. Pauporté, L. Chow, B. Viana, F. Pellé, L. K. Ono, B. Roldan Cuenya, and H. Heinrich, *Appl. Surf. Sci.*, 2010, **256**, 1895–1907.
20. J. B. Cui, Y. C. Soo, T. P. Chen, and U. J. Gibson, *J. Phys. Chem. C*, 2008, **112**, 4475–4479.
21. R. Tena-Zaera, J. Elias, C. Lévy-Clément, C. Bekeny, T. Voss, I. Mora-Seró, and J. Bisquert, *J. Phys. Chem. C*, 2008, **112**, 16318–16323.
22. O. Lupan, T. Pauporté, I. M. Tiginyanu, V. V. Ursaki, V. Şontea, L. K. Ono, B. R. Cuenya, and L. Chow, *Thin Solid Films*, 2011, **519**, 7738–7749.
23. J. Rousset, E. Saucedo, and D. Lincot, *Chem. Mater.*, 2009, **21**, 534–540.
24. T. Pauporté, E. Jouanno, F. Pellé, B. Viana, and P. Aschehoug, *J. Phys. Chem. C*, 2009, **113**, 10422–10431.
25. C. Agashe and S. S. Major, *J. Phys. D. Appl. Phys.*, 1996, **29**, 2988–2991.
26. H. Luo, T. Takata, Y. Lee, J. Zhao, and K. Domen, *Chem. Mater.*, 2004, **16**, 846–849.
27. K. Yang, Y. Dai, B. Huang, and M.-H. Whangbo, *Chem. Mater.*, 2008, **20**, 6528–6534.
28. J. A. Anta, E. Guillén, and R. Tena-Zaera, *J. Phys. Chem. C*, 2012, **116**, 11413–11425.
29. A. V Akimov, A. J. Neukirch, and O. V Prezhdo, *Chem. Rev.*, 2013, **113**, 4496–565.
30. G. Schlichthörl, S. Y. Huang, J. Sprague, and a. J. Frank, *J. Phys. Chem. B*, 1997, **101**, 8141–8155.
31. L. Dloczik, O. Ileperuma, I. Lauermann, L. M. Peter, E. a. Ponomarev, G. Redmond, N. J. Shaw, and I. Uhlendorf, *J. Phys. Chem. B*, 1997, **101**, 10281–10289.
32. F. Fabregat-Santiago, G. Garcia-Belmonte, I. Mora-Seró, and J. Bisquert, *Phys. Chem. Chem. Phys.*, 2011, **13**, 9083–9118.
33. T. Pauporte and J. Rathousky, *J. Phys. Chem. C*, 2007, **111**, 7639–7644.
34. T. Loewenstein, K. Nonomura, T. Yoshida, E. Michaelis, D. Wöhrle, J. Rathousky, M. Wark, and D. Schlettwein, *J. Electrochem. Soc.* , 2006, **153** , A699–A704.
35. T. YANE, A. KOYAMA, K. HIRAMATSU, Y. ISOGAI, K. ICHINOSE, and T. YOSHIDA, *Electrochemistry*, 2012, **80**, 891–897.
36. N. Asakuma, T. Fukui, M. Toki, K. Awazu, and H. Imai, *Thin Solid Films*, 2003, **445**, 284–287.
37. T. Yoshida, J. Zhang, D. Komatsu, S. Sawatani, H. Minoura, T. Pauporté, D. Lincot, T. Oekermann, D. Schlettwein, H. Tada, D. Wöhrle, K. Funabiki, M. Matsui, H. Miura, and H. Yanagi, *Adv. Funct. Mater.*, 2009, **19**, 17–43.
38. H. Graaf, F. Lüttich, C. Dunkel, M. Wark, and T. Oekermann, *J. Phys. Chem. C*, 2012, **116**, 5610–5613.
39. K. Nonomura, D. Komatsu, T. Yoshida, H. Minoura, and D. Schlettwein, *Phys. Chem. Chem. Phys.*, 2007, **9**, 1843–9.
40. K. ICHINOSE, Y. KIMIKADO, and T. YOSHIDA, *Electrochemistry*, 2011, **79**, 146–155.
41. *FIZ Karlsruhe (Germany), Struct. Database ICSD*, 086254.
42. A. Hagfeldt, G. Boschloo, L. Sun, L. Kloo, and H. Pettersson, *Chem. Rev.*, 2010, **110**, 6595–663.
43. J. Halme, P. Vahermaa, K. Miettunen, and P. Lund, *Adv. Mater.*, 2010, **22**, E210–34.
44. J. Bisquert, F. Fabregat-Santiago, I. Mora-Seró, G. Garcia-Belmonte, and S. Giménez, *J. Phys. Chem. C*, 2009, **113**, 17278–17290.
45. J. Rathousky, T. Loewenstein, K. Nonomura, T. Yoshida, M. Wark, and D. Schlettwein, in *Nanoporous Materials IV Proceedings of the 4th International Symposium on Nanoporous Materials*, ed. A. S. and M. J. B. T.-S. in S. S. and Catalysis, Elsevier, 2005, vol. Volume 156, pp. 315–320.